Department of Oncology, Jiangxi Chest Hospital, Nanchang City, P.R. China

The effects of A549 and H1299 cell-derived exosomes on the proliferation and apoptosis of BEAS-2B cells

Zhenbin Li, Xuan Chen, Xiangjun Yi*

Received April 3, 2021, accepted May 1, 2021

**Corresponding author: Xiangjun Yi, Department of Oncology, Jiangxi Chest Hospital, No. 346, Dieshan Road, Donghu District, Nanchang City 330006, Jiangxi Province, P.R. China*
yxj196412@163.com

Pharmazie 76: 379-387 (2021) *doi: 10.1691/ph.2021.1513*

The effects of human non-small cell lung cancer A549 and H1299 cell-derived exosomes on BEAS-2B cell proliferation and apoptosis were investigated. Morphology and size of A549 and H1299 cell-derived exosomes were assessed using transmission electron microscopy and nanoparticle tracking analysis. BEAS-2B cell proliferation, apoptosis and SIRT7 protein expression were determined using CCK8, flow cytometry and Western blot. Transcriptome sequencing, GO analysis, and KEGG pathway analysis were performed. A549 and H1299 cell-derived exosomes demonstrated a microvesicle structure of bilayer membrane with a diameter of about 80 nm. Compared with control, these had no effect on BEAS-2B cell proliferation, but significantly promoted cell apoptosis, and decreased SIRT7 protein expression. Compared with control, A549 cell-derived exosomes have 20 differently expressed genes (10 upregulated, 10 downregulated); 1073 GO terms were enriched, while H1299 cell-derived exosomes have 112 differently expressed genes (80 upregulated, 32 downregulated); 3340 GO terms were enriched. For A549 cell-derived exosomes vs. control, the enriched pathways mainly included dorso-ventral axis formation, endocytosis, endometrial cancer, acute myeloid leukemia, and pathogenic *Escherichia coli* infection. For H1299 cell-derived exosomes vs. control, the enriched pathways mainly included influenza A, herpes simplex infection, measles, TNF signaling pathway, salmonella infection, and Hepatitis C. A total of 608,315 mutation sites were identified, including 553,800 single nucleotide polymorphism sites (SNP) and 54,515 Indel polymorphism sites. The SNP mutation sites were mainly concentrated in A->G, C->T, G->A and T->C. These findings suggested that A549 and H1299 cell-derived exosomes can promote BEAS-2B cell apoptosis by inhibiting SIRT7 expression.

1. Introduction

As one of the most common malignant tumors in the world, lung cancer has seriously threatened human health, and about 85% of lung cancer cases are diagnosed as non-small cell lung cancer (NSCLC) (Wang et al. 2018). Statistics show that the survival rate of lung cancer patients in the recent five years is less than 20% (Siegel et al. 2019). Therefore, in-depth study of the experimental mechanism of the occurrence and development of the NSCLC and the search for new therapeutic targets are of great practical significance for the clinical diagnosis and treatment of lung cancer.
Exosomes are spherical extracellular vesicles with a lipid bilayer membrane structure, and a diameter of 50-100 nm (Théry et al. 2002). Exosomes contain a variety of biologically active molecules, including proteins, nucleic acids and lipids, which play an important role in many pathological and physiological processes, and can transmit signal molecules to other cells to change the functions of the cells, which is an important way of inter-cell information transmission (Colombo et al. 2014). Studies have found that exosomes are involved in the regulation of multiple processes of tumorigenesis, including promoting tumor angiogenesis (Liu et al. 2016), regulating the immune response in the tumor microenvironment (Cai et al. 2012), epithelial-mesenchymal transition (Kim et al. 2016), and promoting tumor cell invasion and metastasis (Gao et al. 2018), which are of great significance in tumor research.
Sirtuin 7 (SIRT7) belongs to the Sirtuin protein family. It is involved in rDNA transcription, protein synthesis, cell survival and lipid metabolism (Kiran et al. 2015). It acts as an oncogene or a tumor suppressor gene, which participates in the proliferation and differentiation, invasion and metastasis, and apoptosis of tumor cells (Malik et al. 2015; Yu et al. 2014). Studies have shown that it is a target of miR-152 and plays a key role in the regulation of aging (Gu et al. 2016).
In this study, we collected human NSCLC cell-derived exosomes (A549 and H1299) and co-cultured with BEAS-2B cells to explore their effects on proliferation and apoptosis of BEAS-2B cells and SIRT7 expression, and used transcriptome sequencing technology to study the differentially expressed genes and revealed the possible mechanisms.

2. Investigations and results

2.1. Identification of exosomes

A549 and H1299 human NSCLC cell-derived exosomes were collected by differential centrifugation. Their morphology and size were evaluated by TEM and NTA (Figs. 1A, 1B), and it was found that the exosomes showed a microvesicle structure with a double-layer membrane of about 80 nm in diameter. Western blot analysis confirmed that the marker proteins CD63 and CD9 were detected in H1299 cell-derived exosomes (Fig. 1C).

2.2. Effect of exosomes on proliferation and apoptosis of BEAS-2B cells

In order to detect the effects of A549 and H1299 cell-derived exosomes on proliferation and apoptosis of BEAS-2B cells, CCK-8 was used to detect the cell viability, and the results are shown in Fig. 2. Compared with the control group, the A549 and H1299 cell-derived exosomes did not affect the proliferation of

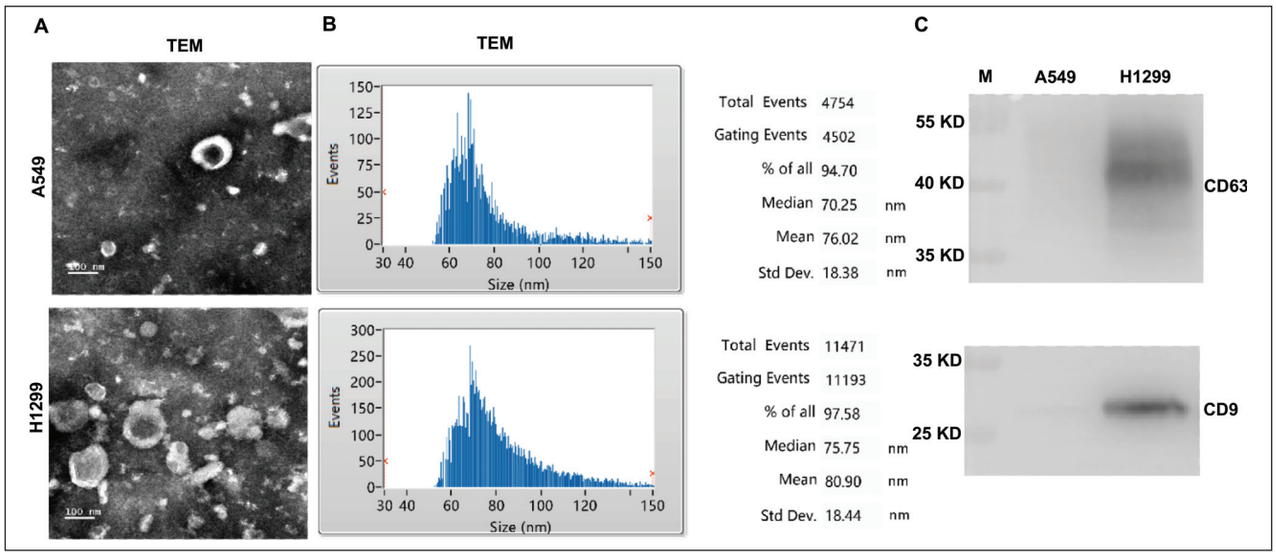

Fig. 1: Exosomes identification. (A) human NSCLC A549 and H1299 cell-derived exosomes observed under TEM (scale bar = 100 nm). (B) results of exosomal nanoparticle tracking analysis (NTA). (C) exosomal related proteins detected by Western blot.

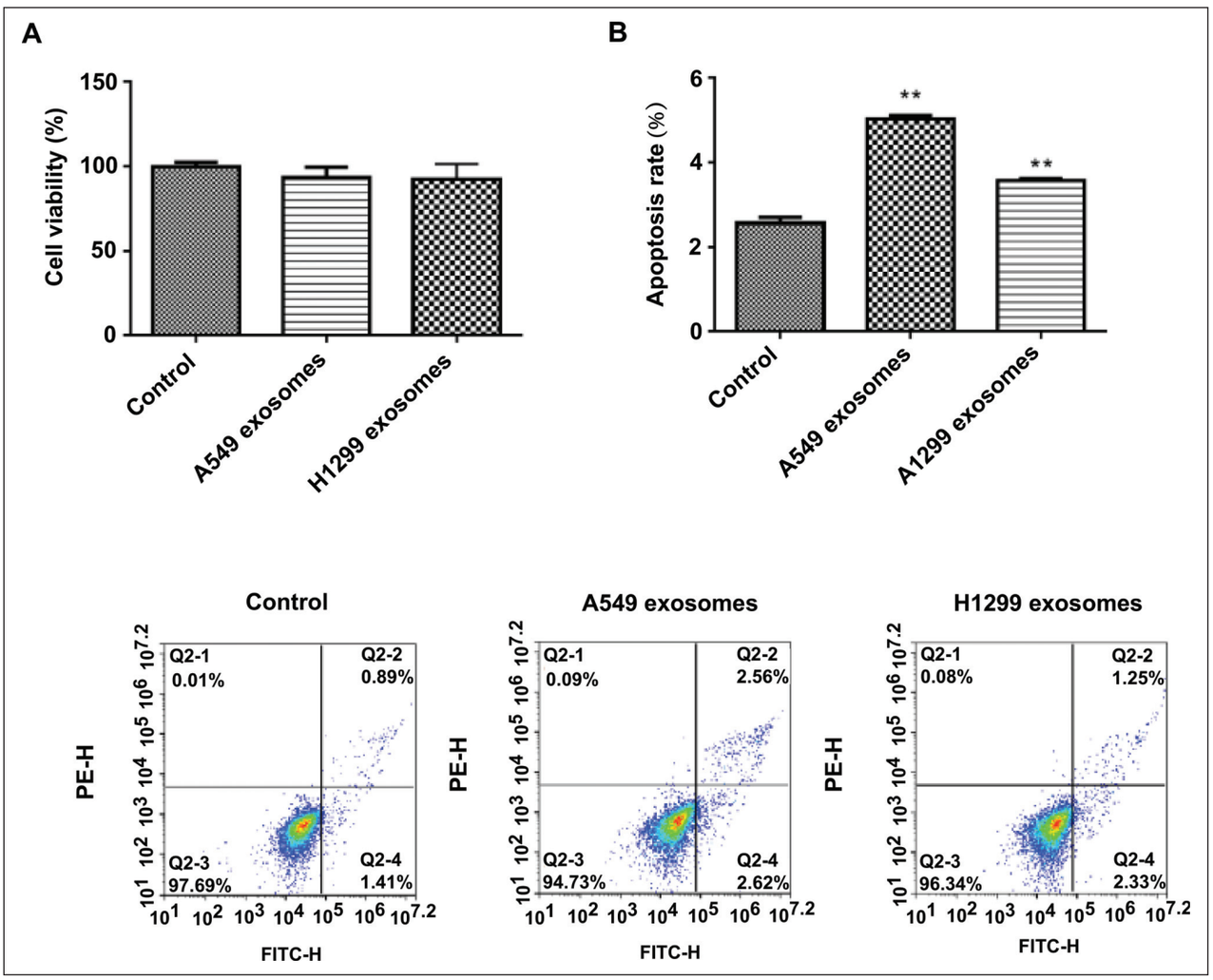

Fig. 2: Effects of A549 and H1299 cell-derived exosomes on proliferation and apoptosis of BEAS-2B cells. (A) cell proliferation detected by CCK-8. (B) cell apoptosis detected by flow cytometry. Data were presented as mean ± SD. **P < 0.01 compared with the control group.

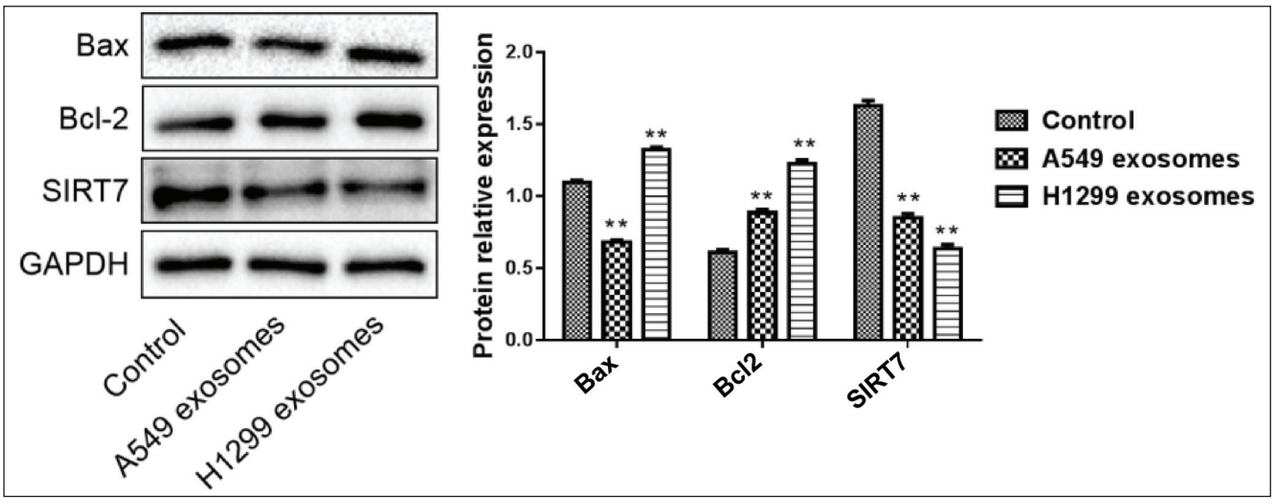

Fig. 3: Bax, Bcl-2 and SIRT7 protein expressions detected by Western blot. Data were presented as mean±SD. **P<0.01 compared with the control group.

BEAS-2B cells (Fig. 2A), but significantly promoted apoptosis (Fig. 2B).

2.3. Effect of exosomes on Bax, Bcl-2 and SIRT7 expressions in BEAS-2B cells

The effects of A549 and H1299 cell-derived exosomes on Bax, Bcl-2 and SIRT7 proteins in BEAS-2B cells were further determined by Western blot, and the results are shown in Fig. 3. Compared with the control group, A549 cell-derived exosomes significantly decreased the Bax and SIRT7 protein expressions, but increased the Bcl-2 protein expression. In addition, the H1299 cell-derived exosomes significantly increased the Bax and Bcl-2 protein expressions, but decreased the SIRT7 protein expression. These results indicate that the A549 and H1299 cell-derived exosomes can promote BEAS-2B cell apoptosis by inhibiting SIRT7 protein expression.

2.4. Dual luciferase verification

Previous studies showed that SIRT7 has binding sites with miR-152, thus through the luciferase reporter gene, we further verified whether SIRT7 also have binding sites with miR-152-3p. The results are shown in Fig. 4. Combination of wild-type SIRT7 (WT) and miR-152-3p mimic can increase luciferase activity, indicating that SIRT7 has no target relationship with miR-152-3p.

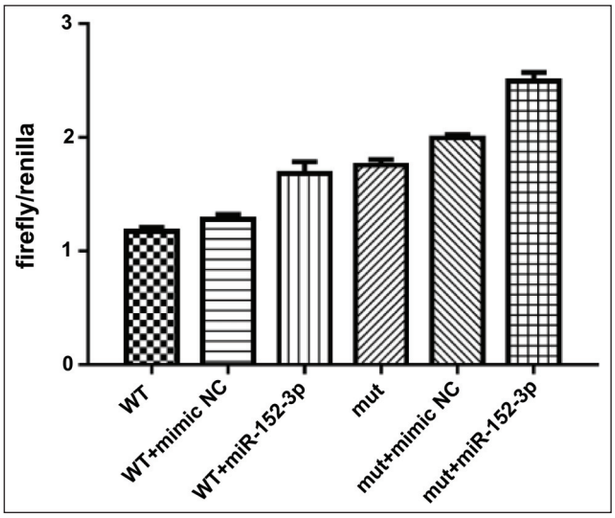

Fig. 4: Dual luciferase verification of the targeting relationship between SIRT7 and miR-152-3p. Data were presented as mean±SD.

2.5. Sequencing data quality control

The data obtained after high-throughput sequencing underwent a series of quality control (FastQC and Trimmomatic for quality cutting), and yielded relatively accurate and effective data. As shown in Table 1A, a total of 471,352,362 sequences were obtained, with an average of 52,372,485 sequences per sample and an average read length of 145.33 bp. The mean data volume of each library was Q20>97%, Q30>89%, and the mean GC content was 48.96%.

HISAT2 software was used to compare the effective data of the sample with the reference genome group and calculate the mapping information. The results are shown in Table 1B. The comparison rate was above 98%.

Table 1. Sequencing data quality control

(A) Summary of data output quality

Sample	Number of sequence	Number of base (bp)	Mean read length (bp)	Q20	Q30	GC
A1	53118556	7715287258	145.25	97.37%	89.94%	48.68%
A2	48578714	7072168270	145.58	97.53%	90.30%	48.31%
A3	55936440	8138998942	145.5	97.51%	90.18%	47.92%
B1	51770270	7513252872	145.13	97.49%	90.44%	52.36%
B2	66528646	9626263509	144.69	97.55%	90.43%	47.88%
B3	49354414	7189079654	145.66	97.63%	90.54%	48.56%
C1	38403872	5580601206	145.31	97.44%	89.95%	48.94%
C2	51973572	7566214655	145.58	97.52%	90.20%	49.10%
C3	55687878	8089263484	145.26	97.40%	89.82%	48.89%

Note: A: control group; B: A549 cells-derived exosome group; C: H1299 cells-derived exosome group

(B) Statistical results of mapping ratio after comparison

Samples	Total reads	Mapped reads	Mapped rate
A1	52949428	52009657	98.23%
A2	48476776	47661863	98.32%
A3	55778230	54809819	98.26%
B1	51549304	50716229	98.38%
B2	66398852	65130946	98.09%
B3	49260066	48462601	98.38%
C1	38307314	37639237	98.26%
C2	55599926	54614420	98.23%
C3	51893412	51005464	98.29%

Note: A: control group; B: A549 cells-derived exosomes group; C: H1299 cells-derived exosomes group

2.6. Differential gene expression analysis

DESeq2 was used for gene expression differential analysis, and the results were visualized. As shown in Table 2A, compared with the control group, A549 cell-derived exosomes have 20 differently expressed genes, of which 10 are upregulated genes (such as interferon alpha-inducible protein 6 (IFI6), interferon-stimulated gene 15 (ISG15), myxovirus resistance 1 (MX1), interferon alpha inducible protein 27 (IFI27), etc.), and 10 are downregulated genes (such as myelin protein zero like 1 (MPZL1), actin-related protein 2/3 complex subunit 5 (ARPC5) and F-actin capping protein alpha-1 subunit (CAPZA1)). Compared with the control group, the H1299 cell-derived exosomes have 112 differently expressed genes, of which 80 are upregulated genes (such as 2'-5'-oligoadenylate synthetase 1 (OAS1), 2'-5'-oligoadenylate synthetase 3 (OAS3), interferon-induced transmembrane protein 3 (IFITM3) and hect domain and RLD 6 (HERC6)), and 32 are downregulated genes (such as mitogen-activated protein kinase 14 (MAPK14), microtubule-associated protein 1S (MAP1S) and myelin protein zero like 1 (MPZL1)). In addition, scatter plots and volcano plots can also reveal the differentially expressed genes between different components (Fig. 5).

2.7. Differential gene GO enrichment analysis

TopGO was used to perform GO enrichment analysis on the differently expressed genes between different components. The results are shown in Table 2B. In the A549 cell-derived exosomes group vs. control group, 1073 GO terms were enriched, mainly including innate immune response, protein polymerization, type I interferon signaling pathway, cellular response to type I interferon, response to type I interferon and regulation of actin filament polymerization (Fig. 6). In the H1299 cell-derived exosomes group vs. control group, 3340 GO terms were enriched, mainly including type I interferon signaling pathway, cellular response to type I interferon, response to type I interferon, response to cytokine, response to virus, and defense response to virus (Fig. 6).

2.8. Differential gene KEGG enrichment analysis

clusterProfiler was used to perform KEGG enrichment analysis on the differentially expressed genes between different components. The results are shown in Fig. 7. In the A549 cell-derived exosomes group vs. control group, the enriched pathways mainly include B cell receptor signaling pathway, dorso-ventral axis formation,

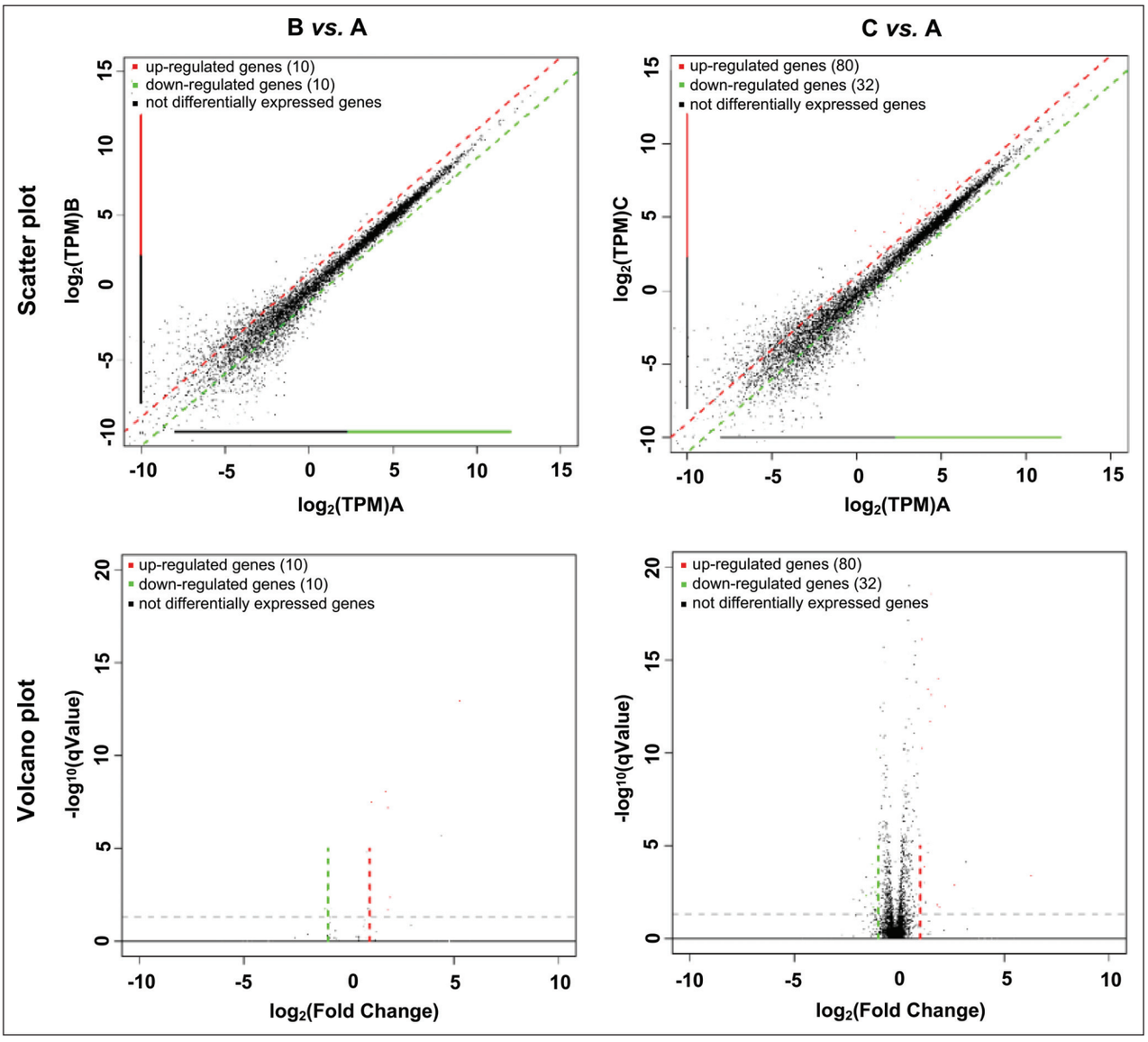

Fig. 5: Scatter plot and volcano plot of the differentially expressed genes between different components. *Note: A: control group; B: A549 cell-derived exosomes group; C: H1299 cell-derived exosomes group. Each dot in the figure represents a specific gene or transcript. The red dots represent genes that are significantly upregulated; the green dots represent genes that are significantly downregulated, and the black dots are non-significantly different genes.

Table 2. Differential gene expression analysis and differential gene GO enrichment analysis

(A) Statistical table of differentially expressed genes (fold-change (FC) ≥ 2 and FDR ≤ 0.05)

Differential gene	All	Up	Down
B *vs.* A	20	10	10
C *vs.* A	112	80	32

Note: A: Control group; B: A549 cells-derived exosomes group; C: H1299 cells-derived exosomes group

(B) Statistical table of GO enrichment analysis of differentially expressed genes among different components (P<0.01)

Sample	GO enrichment number	BP	CC	MF
B *vs.* A	1073	802	156	115
C *vs.* A	3340	2768	240	332

Note: A: control group; B: A549 cells-derived exosomes group; C: H1299 cells-derived exosomes group.

endocytosis, endometrial cancer, acute myeloid leukemia, and pathogenic Escherichia coli infection. In the H1299 cell-derived exosomes group vs. control group, the enriched pathways mainly include influenza A, herpes simplex infection, measles, tumor necrosis factor (TNF) signaling pathway, Salmonella infection, and hepatitis C.

Table 3. SNP and Indel analysis

(A) Statistical analysis table

Samples	SNP	InDel
A1	66446	6543
A2	62773	6281
A3	71390	7074
B1	49062	3928
B2	72150	7572
B3	61057	6098
C1	47225	4819
C2	62356	6191
C3	61341	6009

Note: A: control group; B: A549-cells derived exosomes group; C: H1299-cells derived exosomes group.

2.9 SNP and Indel analysis

Based on the HISAT2 results of comparison between the reads of each sample and the reference genome sequence, the single base mismatches between the sequenced sample and the reference genome were identified; the potential single nucleotide polymorphism (SNP) sites were identified, and whether these SNP sites affect the gene expression level or the type of protein products can then be analyzed. Indel mutation also reflects the difference between the sample and the reference genome, and indel in the coding region will cause frameshift mutation, resulting in changes in gene function. The results are as shown in Table 3A; a total of 608,315 mutation sites were identified, of which SNP was the main mutation site with 553,800 in total, and 54,515 indel polymorphism sites. In addition, SNP mutation sites included transitions (CT and GA) and transversions (CA, GT, CG and AT). It can be seen from Table 3B that the mutation sites of the four groups of samples were mainly concentrated in A->G, C->T, G->A and T->C.

3. Discussion

At present, lung cancer is still the first leading cause of cancer death in the world (Richman et al. 2017). Although good achievements have been made in the diagnosis and treatment of NSCLC, the global control of the disease is still not satisfactory. In recent years, it has been found that the exosomes secreted by NSCLC are the interstitial communication between the tumor cells and mesenchymal cells and play an important role in the occurrence and development of NSCLC (Hoshino et al. 2015; Huang et al. 2013). In this study, we successfully extracted exosomes from A549 and H1299 cells and treated the BEAS-2B cells.

SIRT7, which belongs to the mammalian sirtuin family, plays an important role in carcinogenic transformation (Ford et al. 2006). Li et al. (2018) proved that SIRT7 knockdown inhibits the proliferation and cell cycle progression of HUCCT1 (cholangiocarcinoma) cells *in vitro* and *in vivo*. Some studies have proved that SIRT7 is the target gene of miR-152 (Gu et al. 2016). However, in this study, it was found that SIRT7 has no target relationship with miR-152-3p. Some studies have proved that Sirt7 is a clear target of mir-125 in bladder cancer (Han et al. 2013), while in gastric cancer SIRT7 selectively binds to miR-34a promoter (Zhang et al. 2015). SIRT7 is involved in the regulation of cardiac cell apoptosis and stress response (Araki et al. 2015; Vakhrusheva et al. 2008). In human gastric cancer MGC803 cell line, knocked out SIRT7 upregulated the expression of apoptotic proteins Bax and Bim, indicating that SIRT7 knockout promotes gastric cancer cell apoptosis (Zhang et al. 2015). Similar to previous findings, we found that SIRT7 in BEAS-2B cells was inhibited after treatment with A549 and H1299 cell-derived exosomes, and the BEAS-2B cell apoptosis was inhibited. Therefore, exosomes may inhibit BEAS-2B cell apoptosis by targeting SIRT7.

(B) SNP mutation sites

Samples	A->C	A->T	C->A	C->G	G->C	G->T	T->A	T->G	A->G	C->T	G->A	T->C
A1	1792	1241	1898	2645	2729	1810	1176	1754	16386	9446	9524	16080
A2	1727	1230	1790	2530	2547	1741	1121	1681	15349	8930	9038	15122
A3	1883	1377	2031	2795	2848	1910	1296	1891	17838	9944	10029	17585
B1	1375	773	1414	2272	2274	1402	731	1328	11212	7623	7724	10966
B2	1940	1423	2078	2851	2905	1985	1315	1910	17846	10131	10224	17586
B3	1649	1138	1775	2463	2529	1674	1085	1628	14807	8838	8931	14573
C1	1338	900	1399	1947	2038	1326	844	1315	11123	7029	7186	10808
C2	1648	1161	1762	2504	2549	1695	1089	1668	15355	8853	8954	15159
C3	1646	1130	1717	2485	2520	1661	1095	1609	15167	8689	8793	14864

Note: A: control group; B: A549-cells derived exosomes group; C: H1299-cells derived exosomes group.

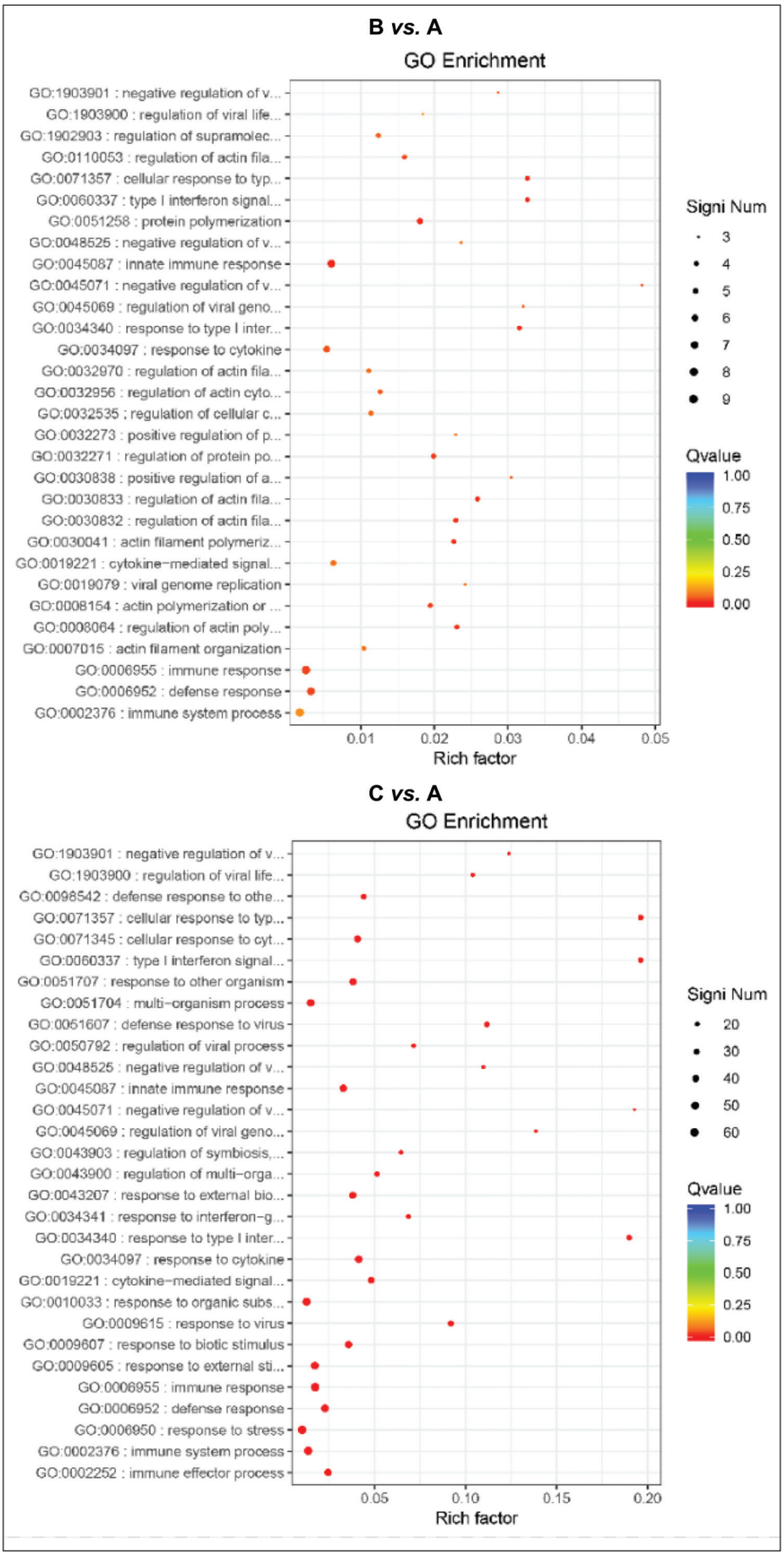

Fig. 6: GO function analysis of the differentially expressed genes enrichment between different components. *Note: A: control group; B: A549 cell-derived exosomes group; C: H1299 cell-derived exosomes group. The horizontal axis represents the enrichment factor, that is, the ratio of the number of differential genes enriched in a certain GO Term to the number of background genes obtained by sequencing. The vertical coordinate represents the function enriched by the GO Term: the larger the circle, the higher the number of differential genes were enriched for this function. The color spectrum from blue to red represents the corrected p-value.

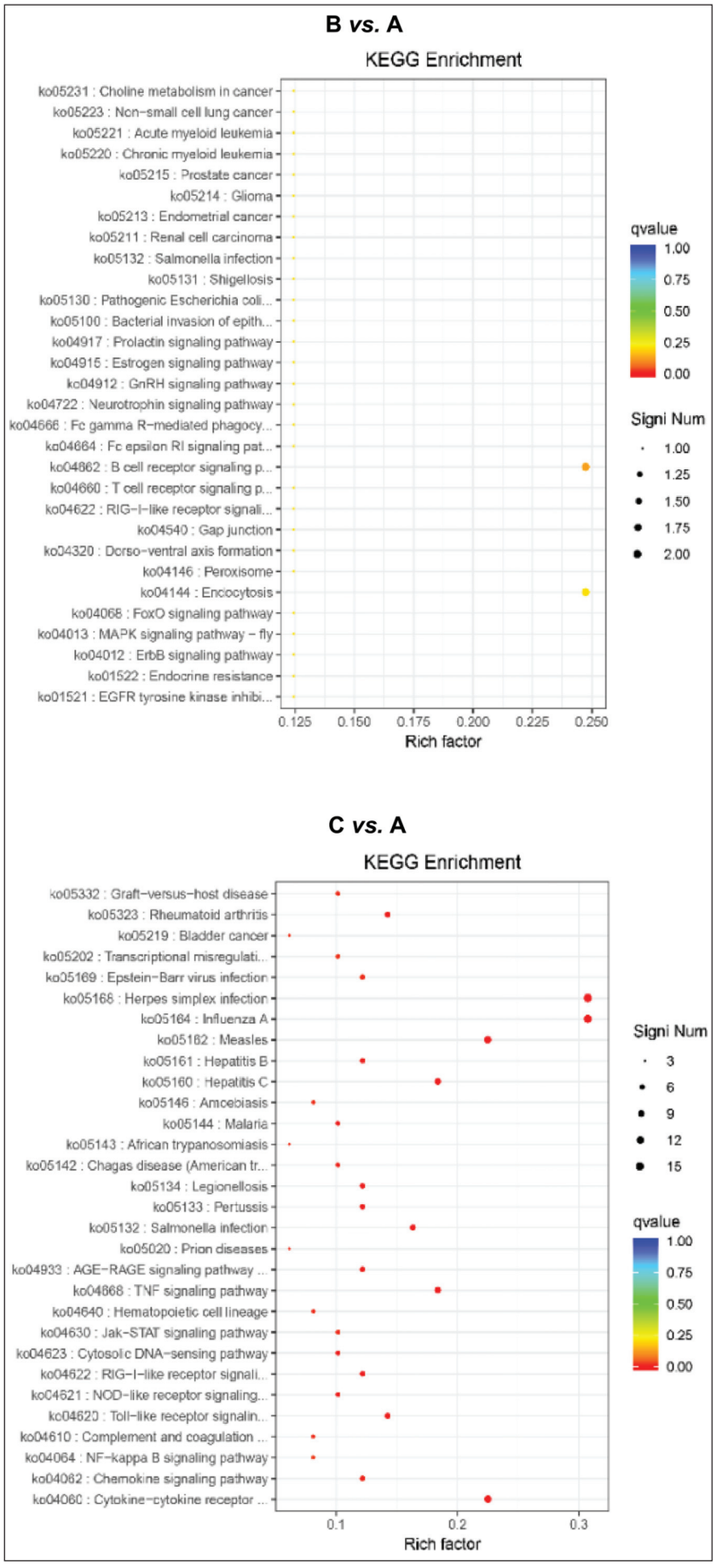

Fig. 7: KEGG function analysis of the differentially expressed genes enrichment between different components. *Note: A: control group; B: A549 cell-derived exosomes group; C: H1299 cell-derived exosomes group. The horizontal axis represents the enrichment factor, that is, the ratio of the number of differential genes enriched in a certain KEGG pathway to the number of background genes obtained by sequencing. The vertical coordinate represents the function enriched by the KEGG pathway: the larger the circle, the higher the number of differential genes enriched in this pathway. The color spectrum from blue to red represents the corrected p-value.

Comparative analysis of differential gene expression is a technique to identify the gene expression and differential gene expression between tissues or cells at the transcriptional level. It is the most effective way to explain the mechanism of biological development and differentiation. It has been widely used in the field of disease-related gene isolation and is one of the core fields of genomics research. This study conducted a preliminary research on the mechanism of the effect of NSCLC cell-derived exosomes on normal cells from the perspectives of differentially expressed genes and biological signaling pathways. KEGG annotation and cluster analysis showed that the differentially expressed genes were significantly enriched in signal transduction pathways, mainly B-cell receptor signaling pathway, TNF signaling pathway and various disease-related pathogenic pathways, such as endometrial cancer signaling pathway, HSV-1 signaling pathway and Hepatitis C signaling pathway. Most of them were related to the phosphatidylinositol 3-kinase (PI3K)/protein kinase B (Akt) signaling pathway and MAPK signaling pathway. PI3K/Akt signaling pathway is closely related to the occurrence of common cancers (Fresno et al. 2004; Xu et al. 2015). MAPK signaling plays a key role in oxidative stress, DNA damage and cancer progression (Rezatabar et al. 2019), suggesting that these two pathways play an important role in NSCLC. Using DESeq2 for differential gene expression analysis, in A549 cell-derived exosomes vs. control group, 20 differentially expressed genes were found, of which 10 were upregulated genes, mainly including IFI6 and ISG15, and 10 were downregulated genes, such as MPLZ1 and ARPC5. These genes have been proved to play important roles in many biological functions such as anti-viral, anti-apoptosis and anti-tumor activities (Chen et al. 2019; Han et al. 2018; Xiong and Luo 2018). In H1299 cell-derived exosomes vs. control group, there were 112 differentially expressed genes, of which 80 were upregulated genes and 32 were downregulated genes. Some studies have found that lung cancer cell-derived exosomes affect the immune mechanism of lung cancer, mainly through the change of immunosuppression to protect the tumor. It can also activate and increase regulatory T cells and suppressor cells and inhibit CD8+ T cell-mediated tumor targeting immunity (Cocucci and Meldolesi 2015). In addition, it was also found that exosomes can directly induce CD8+ T cell apoptosis (Stenqvist et al. 2013).

Thus, the present study demonstrated that human NSCLC A549 and H1299 cell-derived exosomes significantly decreased SIRT7 protein expression in BEAS-2B cells and significantly promoted cell apoptosis, but had no effect on cell proliferation. The differential expression analysis showed that it is associated with some pathways which are related to tumorigenesis, such as PI3K/Akt signaling pathway and MAPK signaling pathway, and it was found that NSCLC cell-derived exosomes mainly played a role in the immune response during invasion into normal cells. This study is of great significance for further study the mechanism of tumor cell exosomes, yet further experimental validation is still needed.

4. Experimental

4.1. Main reagents

A549 cells, H1299 cells, BEAS-2B cells, 293T cells (BeNa Culture Collection, Beijing, P.R. China); Roswell Park Memorial Institute (RPMI)-1640 complete medium, 1× phosphate buffer saline (PBS), Cell Counting Kit (CCK)-8 cell proliferation detection kit (KeyGen Biotech Co., Ltd, Nanjing, Jiangsu, P.R. China); Gibco® RPMI 1640 medium, GlutaMAX (Thermo Fischer Scientific Inc., Waltham, MA, USA); trypsin-ethylenediamine tetraacetic acid (EDTA) digestion solution, 30% acrylamide (Beijing Solarbio Science and Technology Co. Ltd., Beijing, P.R. China); fetal bovine serum (FBS) (Biological Industries, Shanghai, P.R. China); CD9, CD63 (Abcam plc, Cambridge, UK); Annexin V-fluorescein isothiocyanate (FITC)/propidium iodide (PI) apoptosis kit (Hangzhou MultiSciences (Lianke) Biotech, Co., Ltd., Hangzhou, Zhejiang, P.R. China); lipofectamine 3000 transfection reagent (Invitrogen Corp., Carlsbad, CA, USA); dual-luciferase reporter gene assay kit (Beyotime Biotechnology, Shanghai, P.R. China); radioimmunoprecipitation assay (RIPA) cell lysis buffer (Applygen Technologies Inc., Beijing, P.R. China); sodium dodecyl sulfate (SDS) (Xilong Scientific Co., Ltd., Guangdong, P.R. China); bicinchoninic acid (BCA) protein assay kit (Beijing Cowin Bioscience Co. Ltd., Beijing, P.R. China); enhanced chemiluminescence (ECL) Plus (Thermo Fisher Scientific, Waltham, MA, USA); internal control primary antibody: mouse monoclonal anti-glyceraldehyde 3-phosphate dehydrogenase (GAPDH) (1:2000) (Zsbio Commerce Store, Beijing, P.R. China), secondary antibody: goat anti-mouse immunoglobulin G (IgG) (H+L) antibody horseradish peroxidase (HRP) conjugate (1:2000) (Zsbio Commerce Store, Beijing, P.R. China); target primary antibodies: rabbit anti-SIRT7 (1:500) (Proteintech Group, Inc., Rosemont, IL, USA), rabbit anti-B-cell lymphoma (Bcl)-2 (1:1000) (Bioss Inc., Woburn, MA, USA), rabbit anti-Bax (1:1000) (Abcam plc, Cambridge, UK), secondary antibody: goat anti-rabbit IgG (H+L) antibody HRP conjugate (1:2000) (Zsbio Commerce Store, Beijing, P.R. China).

4.2. Main instruments

Ultra-high sensitivity chemiluminescence imaging system (Chemi DocTM XRS+, Bio-Rad Laboratories, Inc., Shanghai, P.R. China); automated microplate reader; NovoCyteTM flow cytometer (NovoCyte 2060R, ACEA BIO (Hangzhou) Co., Ltd., Zheqiang, P.R. China); transmission electron microscope (TEM) (Jeol, JEM-1230 (80 kV), Tokyo, Japan); ultracentrifuge (Optima L-100XP, Beckman Coulter, Inc., Brea, CA, USA).

4.3. Isolation and identification of exosomes

The human NSCLC cells (A549 and H1299) were cultured until the number was sufficient. The incomplete medium was replaced. The cell supernatant was collected after 48 h of starvation, and the exosomes were collected by differential centrifugation. The supernatant was centrifuged at 2000 × for 30 min at 4 °C, then carefully transferred to a new centrifuge tube and recentrifuged at 12,000 × g for 45 min at 4 °C to remove larger vesicles. The supernatant was taken and filtered through a 0.45 μm filter membrane. The filtrate was collected and transferred to a new centrifuge tube. An ultra-speed rotor was selected, and centrifuged at 110,000 × g for 70 min at 4 °C. The supernatant was discarded and resuspended in 10 ml of pre-cooled 1x PBS. An ultra-speed rotor was selected, and ultracentrifugation was repeated at 4 °C, 110,000 × g for 70 min. The supernatant was discarded and resuspended in 100 μl of pre-cooled 1x PBS for 60 min. Subsequently, the morphology and size of the exosomes were detected by TEM and nanoparticle tracking analysis (NTA). In addition, the expressions of exosomes-related proteins calnexin, CD63 and CD9 were detected with Western blot.

4.4. Cell culture

Human NSCLC cells (A549 and H1299) and human lung epithelial cells BEAS-2B were cultured in RPMI-1640 complete medium containing 10% FBS and 1% double antibody. When the cell density reached 80–90%, they needed to be passaged. The cell culture supernatant was discarded, washed twice with 1x PBS, and added 0.25% trypsin (containing 0.02% EDTA) for digestion. After the cells became round, medium was added to terminate digestion. The cell suspension was collected into a 10 ml centrifuge tube, and centrifuged at 1000 rpm for 3 min. Then, the supernatant was discarded and medium was added to resuspend the cells. The cell suspension was divided into a ratio of 1:3 in the prepared culture dish, marked and placed in the incubator for culture. After the cells were fully adhered to the wall, the supernatant was discarded and A549 and H1299 cell-derived exosomes (50 ng/ml) were added respectively, and co-cultured for 24 h.

4.5. Cell viability detected by CCK8

After co-cultured for 24 h, cell proliferation was detected with CCK8 detection kit. Each well was incubated with 10 μl CCK8 detection reagent at 37 °C for 2 h. The OD value of each well was detected with the microplate reader at 450 nm wavelength to calculate cell viability.

4.6. Apoptosis detected by flow cytometry

After co-cultured for 24 h, the cells were digested with trypsin. Then, the cells were collected, and the density was adjusted to 1-3 x 10^6/ml. The cells were then resuspended with binding buffer. Subsequently, 3 μl Annexin V-FITC and 5 μl PI-PE solutions were added to each tube, gently mixed, and incubated at room temperature (RT) for 10 min in the dark. Cell apoptosis was detected by flow cytometry.

4.7. Western blot detection

After co-cultured for 24 h, the cells were collected and added with lysis buffer. The cells were lysed on ice for 30 min and centrifuged at 12000 rpm for 10 min. The supernatant was carefully aspirated for total protein. The protein concentration was determined with BCA kit. Then, the protein was denatured, loaded, and subjected to SDS-polyacrylamide gel electrophoresis (PAGE) for 2 h. Subsequently it was transferred to the membrane with a constant current of 300 mA for 80 min and incubated in primary antibody solution at 4 °C overnight, followed by secondary antibody solution at RT for 2 h. Drops of ECL exposure solution was added onto the membrane, and then exposed using the gel imaging system. The gray value of each antibody band was analyzed using the "ImageJ" software.

4.8. Dual luciferase reporter gene experiment

293T cells were transfected with pRL-SV40 containing 3'-UTR of SIRT7 wild type (WT) and mutant (MUT) on a 12 well plate with or without 25 nM miR-152-3p mimic. The cells were harvested 48 h after transfection and lysed at 4 °C for 20 min using the dual luciferase reporter gene detection kit according to the manufacturer's protocol. For each group, 70 μl of cell lysis buffer was added to a 96-well plate, and 100 μl luciferase assay reagent was added to each well to detect the firefly luciferase activity, followed by 100 μl Renilla luciferase assay reagent (detection substrate:

buffer = 1:100) to detect the Renilla luciferase activity. Renilla luciferase was used for standardization.

4.9. High throughput sequencing of mRNA

After the exosomes were co-cultured for 24 h, the cells were collected, and total RNA was extracted to construct the sequencing library. Sequencing analysis was performed on Illumina Hiseq 4000 sequencing platform and sent to Sangon Biotech (Shanghai) Co., Ltd., Shanghai, P.R. China for processing.

4.10. Quality inspection of sequencing results

Since the raw reads of Illumina Hiseq contain sequencing of adapter sequences, low-quality reads and high N rate sequences, this will seriously affect the quality of subsequent sequence assembly. High-quality sequencing data (clean reads) can be obtained by performing data processing via Trimmomatic. Hierarchical indexing for spliced alignment of transcripts(HISAT)2 software was used to compare the high-quality sequencing sequence obtained after quality control with the designated reference genome. The sequence alignment determines the distribution of reads on the reference genome, which is the basis for subsequent analysis of the gene expression levels.

4.11. Differential gene expression analysis

Based on the fragments per kilo base per million mapped reads (FPKM) calculation formula, the differential expression between two samples was calculated using the Cuffdiff software. All samples were compared in pairs. In order to visualize the overall situation of differential genes among the comparison groups, we used volcano plot to intuitively understand the overall distribution of differential genes. For comparison group without biological duplication, in order to eliminate biological variation, we set thresholds to screen the differential genes from two aspects: the fold change and significance level at |log2 (fold change)|> 1 and q value <0.05).

4.12. Differential gene gene ontology (GO) and Kyoto encyclopedia of genes and genomes (KEGG) enrichment analysis

The topGO software was used for enrichment analysis, and the method used was Fisher's exact test. In order to control the false positive rate calculation, four multiple test methods (Bonferroni, Holm, Sidak and false discovery rate) were used to correct the p value. Generally, when the false discovery rate adjusted P value (pFDR) ≤ 0.05, it was considered that there was significant enrichment of the GO function.
The clusterProfiler was used to perform KEGG pathway enrichment analysis, and the method used was Fisher's exact test. The calculation principle was the same as GO functional enrichment analysis. In order to control the false positive rate calculation, the Benjamini-Hochberg (BH) FDR method was used for multiple tests. The calculation formula was the same as the previous section. The corrected p-value was set to 0.05 as the threshold. The KEGG pathway that met this condition was defined as the significant enriched pathway of the differentially expressed genes.

4.13. Gene structure analysis

BCFtools was used to perform single-nucleotide polymorphism (SNP)/insertion or deletion (Indel) calling according to the mapping results, and the SNP/Indel in each sample was extracted. Then, SnpEff was used to calculate the distribution of variant sites on the genome structure. It was filtered according to the following conditions: 1) the quality value was greater than 20; 2) the coverage was greater than 8.

4.14. Statistical analysis

All data were statistically analyzed with GraphPad Prism7 and expressed as mean ± SD. The significant difference between groups was analyzed by analysis of variance (ANOVA), with P<0.05 regarded as significant difference.

Conflicts of interest: None declared.

References

Araki S, Izumiya Y, Rokutanda T, Ianni A, Hanatani S, Kimura Y, Onoue Y, Senokuchi T, Yoshizawa T, Yasuda O, Koitabashi N, Kurabayashi M, Braun T, Bober E, Yamagata K, Ogawa H (2015) Sirt7 contributes to myocardial tissue repair by maintaining transforming growth factor-β signaling pathway. Circulation 132: 1081–1093.

Cai Z, Yang F, Yu L, Yu Z, Jiang L, Wang Q, Yang Y, Wang L, Cao X, Wang J (2012) Activated T cell exosomes promote tumor invasion via Fas signaling pathway. J Immunol 188: 5954–5961.

Chen D, Cao L, Wang X (2019) MPZL1 promotes tumor cell proliferation and migration via activation of Src kinase in ovarian cancer. Oncol Rep 42: 679–687.

Cocucci E, Meldolesi J (2015) Ectosomes and exosomes: shedding the confusion between extracellular vesicles. Trends Cell Biol 25: 364–372.

Colombo M, Raposo G, Théry C (2014) Biogenesis, secretion, and intercellular interactions of exosomes and other extracellular vesicles. Annu Rev Cell Dev Biol 30: 255–289.

Ford E, Voit R, Liszt G, Magin C, Grummt I, Guarente L (2006) Mammalian Sir2 homolog SIRT7 is an activator of RNA polymerase I transcription. Genes Dev 20: 1075–1080.

Fresno Vara JA, Casado E, de Castro J, Cejas P, Belda-Iniesta C, González-Barón M (2004) PI3K/Akt signalling pathway and cancer. Cancer Treat Rev 30: 193–204.

Gao J, Qiu X, Li X, Fan H, Zhang F, Lv T, Song Y (2018) Expression profiles and clinical value of plasma exosomal Tim-3 and Galectin-9 in non-small cell lung cancer. Biochem Biophys Res Commun 498: 409–415.

Gu S, Ran S, Liu B, Liang J (2016) miR-152 induces human dental pulp stem cell senescence by inhibiting SIRT7 expression. FEBS Lett 590: 1123–1131.

Han Y, Liu Y, Zhang H, Wang T, Diao R, Jiang Z, Gui Y, Cai Z (2013) Hsa-miR-125b suppresses bladder cancer development by downregulating oncogene SIRT7 and oncogenic long noncoding RNA MALAT1. FEBS Lett S0014-5793(13)00780-1

Han HG, Moon HW, Jeon YJ (2018) ISG15 in cancer: Beyond ubiquitin-like protein. Cancer Lett 438: 52–62.

Hoshino A, Costa-Silva B, Shen TL, et al (2015) Tumour exosome integrins determine organotropic metastasis. Nature 527: 329–335.

Huang SH, Li Y, Zhang J, Rong J, Ye S (2013) Epidermal growth factor receptor-containing exosomes induce tumor-specific regulatory T cells. Cancer Invest 31: 330–335.

Kim J, Kim TY, Lee MS, Mun JY, Ihm C, Kim SA (2016) Exosome cargo reflects TGF-β1-mediated epithelial-to-mesenchymal transition (EMT) status in A549 human lung adenocarcinoma cells. Biochem Biophys Res Commun 478: 643–648.

Kiran S, Anwar T, Kiran M, Ramakrishna G (2015) Sirtuin 7 in cell proliferation, stress and disease: Rise of the Seventh Sirtuin!. Cell Signal 27: 673–682.

Li W, Sun Z, Chen C, Wang L, Geng Z, Tao J (2018) Sirtuin7 has an oncogenic potential via promoting the growth of cholangiocarcinoma cells. Biomed Pharmacother 100: 257–266.

Liu Y, Luo F, Wang B, Li H, Xu Y, Liu X, Shi L, Lu X, Xu W, Lu L, Qin Y, Xiang Q, Liu Q (2016) STAT3-regulated exosomal miR-21 promotes angiogenesis and is involved in neoplastic processes of transformed human bronchial epithelial cells. Cancer Lett 370: 125–135.

Malik S, Villanova L, Tanaka S, Aonuma M, Roy N, Berber E, Pollack JR, Michishita-Kioi E, Chua KF (2015) SIRT7 inactivation reverses metastatic phenotypes in epithelial and mesenchymal tumors. Sci Rep 5: 9841.

Rezatabar S, Karimian A, Rameshknia V, Parsian H, Majidinia M, Kopi TA, Bishayee A, Sadeghinia A, Yousefi M, Monirialamdari M, Yousefi B (2019) RAS/MAPK signaling functions in oxidative stress, DNA damage response and cancer progression. J Cell Physiol doi: 10.1002/jcp.28334.

Richman DM, Tirumani SH, Hornick JL, Fuchs CS, Howard S, Krajewski K, Ramaiya N, Rosenthal M (2017) Beyond gastric adenocarcinoma: Multimodality assessment of common and uncommon gastric neoplasms. Abdom Radiol (NY) 42: 124–140.

Siegel RL, Miller KD, Jemal A (2019) Cancer statistics, 2019. CA Cancer J Clin 69: 7–34.

Stenqvist AC, Nagaeva O, Baranov V, Mincheva-Nilsson L (2013) Exosomes secreted by human placenta carry functional Fas ligand and TRAIL molecules and convey apoptosis in activated immune cells, suggesting exosome-mediated immune privilege of the fetus. J Immunol 191: 5515–5523.

Théry C, Zitvogel L, Amigorena S (2002) Exosomes: composition, biogenesis and function. Nat Rev Immunol 2: 569–579.

Vakhrusheva O, Smolka C, Gajawada P, Kostin S, Boettger T, Kubin T, Braun T, Bober E (2008) Sirt7 increases stress resistance of cardiomyocytes and prevents apoptosis and inflammatory cardiomyopathy in mice. Circ Res 102: 703–710.

Wang Z, Zheng Y, Fang Z (2018) The clinical efficacy and safety of paclitaxel combined with avastin for NSCLC patients diagnosed with malignant pleural effusion. Rev Assoc Med Bras 64: 230–233.

Xiong T, Luo Z (2018) The expression of actin-related protein 2/3 complex subunit 5 (ARPC5) expression in multiple myeloma and its prognostic significance. Med Sci Monit 24: 6340–6348.

Xu W, Yang Z, Lu N (2015) A new role for the PI3K/Akt signaling pathway in the epithelial-mesenchymal transition. Cell Adh Migr 9: 317–324.

Yu H, Ye W, Wu J, Meng X, Liu RY, Ying X, Zhou Y, Wang H, Pan C, Huang W (2014) Overexpression of sirt7 exhibits oncogenic property and serves as a prognostic factor in colorectal cancer. Clin Cancer Res 20: 3434–3445.

Zhang S, Chen P, Huang Z, Hu X, Chen M, Hu S, Hu Y, Cai T (2015) Sirt7 promotes gastric cancer growth and inhibits apoptosis by epigenetically inhibiting miR-34a. Sci Rep 5: 9787.